

Oriented Image Foresting Transform Segmentation: Connectivity Constraints with Adjustable Width

Lucy A. C. Mansilla, Paulo A. V. Miranda

Department of Computer Science,

University of São Paulo (USP),

05508-090, São Paulo, SP, Brazil.

Email: lucyacm@vision.ime.usp.br, pmiranda@vision.ime.usp.br

Abstract—In this work, we extend a novel seed-based segmentation algorithm, which provides global optimum solutions according to a graph-cut measure, subject to high-level boundary constraints: The simultaneously handling of boundary polarity and connectivity constraints. The proposed method incorporates the connectivity constraint in the Oriented Image Foresting Transform (OIFT), ensuring the generation of connected objects, but such that the connection between its internal seeds is guaranteed to have a user-controllable minimum width. In other frameworks, such as the min-cut/max-flow algorithm, the connectivity constraint is known to lead to NP-hard problems. In contrast, our method conserves the low complexity of the OIFT algorithm. In the experiments, we show improved results for the segmentation of thin and elongated objects, for the same amount of user interaction. Our dataset of natural images with true segmentation is publicly available to the community.

Keywords—image segmentation; connectivity constraints; boundary polarity; image foresting transform

I. INTRODUCTION

Image segmentation is one of the most fundamental and challenging problems in image processing and computer vision. In this work, we focus on seed-based methods for interactive image segmentation [1], [2], [3], [4], [5], where the user provides a partial labeling by drawing scribbles on the image (seed pixels). A graph derived from the image is then partitioned among the different labeled seeds according to some energy formulation, which can be roughly described in a unified manner according to a common framework, sometimes referred to as, Generalized Graph Cut (GGC) [6], [7]. Within this framework, there are two important classes of energy formulations, the ε_1 - and ε_∞ -minimization problems [6], the former including the *min-cut/max-flow* algorithm [2], whereas the latter class encompasses methods, such as *watersheds* [5], *fuzzy connectedness* [4], and *image foresting transform* (IFT) [8].

Global properties such as shape constraints and boundary polarity, are potentially useful high-level priors for object segmentation, allowing the customization of the segmentation to a given target object [9]. The Connectedness is an important global topology property, which can be used as a high-level prior for object segmentation. The seed-based methods can be classified into three groups, according to their level of Connectedness:

- 1) In the first group, we have methods that do not guarantee any level of connectedness (Figures 1a-b). In the graph cut (GC) community, this is usually referred to as the disconnection problem of GC, when the source and sink nodes are connected to all image pixels [2].
- 2) In the second group, we have methods that guarantee that object's pixels are connected to some internal seed. However, note that the object could be composed by several disconnected components, as long as we have some object's seeds in each component (Figure 1c). The majority of methods belong to this class, including fuzzy connectedness and watershed from markers [4], [5].
- 3) In the third group, we have methods that guarantee that the segmented object forms a single connected component in the image domain [10], [11], [12], [9]. This is especially important when the target is a single object (Figure 1d).

In this work, we use the term connectivity constraint to indicate methods from the third group. The ε_1 -minimization among all objects satisfying the connectivity constraint was proved to be NP-Hard [10], [11]. Vicente et al. [10] propose a heuristic algorithm, named *DijkstraGC*, which merges the Dijkstra algorithm and graph cut. *DijkstraGC* is still slow, since it requires many calls to the maxflow algorithm. Other method, named *Topology cuts*, by Zeng et al. [11] also finds only an approximate solution to incorporate topology priors in the min-cut/max-flow algorithm. Nowozin and Lampert adopted a different approach solving a related optimization problem, which forces the output labeling to be connected in the framework of recent maximum a posteriori (MAP)-MRF linear program (LP) relaxations [12], [9].

More recently, Mansilla et al. [13] introduced the connectivity constraint in the ε_∞ -minimization problem of the GGC framework, motivated by the recent advances that have been made in this class, such as the introduction of shape constraints [14], [15] and boundary polarity [16], [17]. Their algorithm, named *Connected Oriented Image Foresting Transform* (COIFT) [13], provides global optimum solutions to the ε_∞ -minimization problem, subject to high-level boundary constraints (polarity and connectivity constraints), conserving the low complexity of the IFT algorithm. Nevertheless, it provides undesirable results with only thin connections in



Fig. 1. (a) Input image with user selected seeds. (b) Segmentation by Graph cut showing the disconnection problem of an object region that is not marked by any seed on the right. (c) Segmentation by IFT resulting in disconnected components that are all marked by some object seed. (d) Segmentation by the proposed method producing a single connected component.

several cases, mitigating its potential positive effects (see the third column of Figure 2). In this work, we extend COIFT in order to guarantee an optimal solution to the ε_∞ -minimization problem (which will be presented here in its equivalent dual form as a maximization problem), under the constraint that the connection between its internal seeds must have a minimum selected width. The width parameter can be controlled by the user to best fit to the object properties (Figure 2). We also discuss how to improve the handling of ties in COIFT energy formulation.

In Section II, we review IFT and OIFT. COIFT is then presented with the proposed extension in Section III. In Section IV, we evaluate the COIFT extension, which subsumes the original COIFT [13] as a particular case, and our conclusions are stated in Section V.

II. IMAGE GRAPH CONCEPTS

A multi-dimensional and multi-spectral image \hat{I} is a pair $\langle \mathcal{I}, \vec{I} \rangle$, where $\mathcal{I} \subset \mathbb{Z}^n$ is the image domain and $\vec{I}(t)$ assigns a set of m scalars $I_i(t)$, $i = 1, 2, \dots, m$, to each pixel $t \in \mathcal{I}$. The subindex i is removed when $m = 1$.

An image can be interpreted as a weighted digraph $G = \langle \mathcal{V}, \mathcal{A}, \omega \rangle$, whose nodes \mathcal{V} are the image pixels in its image domain $\mathcal{I} \subset \mathbb{Z}^n$, and whose arcs are the ordered pixel pairs $\langle s, t \rangle \in \mathcal{A}$. For example, one can take \mathcal{A} to consist of all pairs of ordered pixels $\langle s, t \rangle$ in the Cartesian product $\mathcal{I} \times \mathcal{I}$ such that $d(s, t) \leq \rho$ and $s \neq t$, where $d(s, t)$ denotes the Euclidean distance and ρ is a specified constant (e.g., 4-neighborhood, when $\rho = 1$, and 8-neighborhood, when $\rho = \sqrt{2}$, in case of 2D images). The digraph G is symmetric if for any of its arcs $\langle s, t \rangle \in \mathcal{A}$, the pair $\langle t, s \rangle$ is also an arc of G . Each arc $\langle s, t \rangle \in \mathcal{A}$ has a weight $\omega(\langle s, t \rangle)$, such as a dissimilarity measure between pixels s and t (e.g., $\omega(\langle s, t \rangle) = |I(t) - I(s)|$ for a single channel image with values given by $I(t)$).

The transpose $G^T = \langle \mathcal{V}, \mathcal{A}^T, \omega^T \rangle$ of a weighted digraph $G = \langle \mathcal{V}, \mathcal{A}, \omega \rangle$ is the unique weighted digraph on the same set of vertices \mathcal{V} with all of the arcs reversed compared to the orientation of the corresponding arcs in G (i.e., for any of its arcs $\langle s, t \rangle \in \mathcal{A}^T$, the pair $\langle t, s \rangle$ is an arc of G , and $\omega^T(\langle s, t \rangle) = \omega(\langle t, s \rangle)$).

For a given image graph $G = \langle \mathcal{V}, \mathcal{A}, \omega \rangle$, a path $\pi = \langle t_1, t_2, \dots, t_n \rangle$ is a sequence of adjacent pixels (i.e., $\langle t_i, t_{i+1} \rangle \in \mathcal{A}$, $i = 1, 2, \dots, n-1$) with no repeated ver-

tices ($t_i \neq t_j$ for $i \neq j$). Other greek letters, such as τ , can also be used to denote different paths. A path $\pi_t = \langle t_1, t_2, \dots, t_n = t \rangle$ is a path with terminus at a pixel t . When we want to explicitly indicate the origin of the path, the notation $\pi_{s \rightsquigarrow t} = \langle t_1 = s, t_2, \dots, t_n = t \rangle$ may also be used, where s stands for the origin and t for the destination node. More generally, we can use $\pi_{\mathcal{S} \rightsquigarrow t} = \langle t_1, t_2, \dots, t_n = t \rangle$ to indicate a path with origin restricted to a set \mathcal{S} (i.e., $t_1 \in \mathcal{S}$). A path is *trivial* when $\pi_t = \langle t \rangle$. A path $\pi_t = \pi_s \cdot \langle s, t \rangle$ indicates the extension of a path π_s by an arc $\langle s, t \rangle$.

A *predecessor map* is a function P that assigns to each pixel t in \mathcal{V} either some other adjacent pixel in \mathcal{V} , or a distinctive marker *nil* not in \mathcal{V} — in which case t is said to be a *root* of the map. A *spanning forest* is a predecessor map which contains no cycles — i.e., one which takes every pixel to *nil* in a finite number of iterations. For any pixel $t \in \mathcal{V}$, a spanning forest P defines a path π_t^P recursively as $\langle t \rangle$ if $P(t) = \text{nil}$, and $\pi_s^P \cdot \langle s, t \rangle$ if $P(t) = s \neq \text{nil}$.

A. Image Foresting Transform (IFT)

A *connectivity function* computes a value $f(\pi_t)$ for any path π_t , usually based on arc weights. A path π_t is *optimum* if $f(\pi_t) \leq f(\tau_t)$ for any other path τ_t in G . By taking to each pixel $t \in \mathcal{V}$ one optimum path with terminus at t , we obtain the optimum-path value $V_{opt}^f(t)$, which is uniquely defined by $V_{opt}^f(t) = \min_{\pi_t \in G} \{f(\pi_t)\}$. The *image foresting transform* (IFT) [8] takes an image graph $G = \langle \mathcal{V}, \mathcal{A}, \omega \rangle$, and a path-cost function f ; and assigns one optimum path to every pixel $t \in \mathcal{V}$ such that an *optimum-path forest* P is obtained — i.e., a spanning forest where all paths π_t^P for $t \in \mathcal{V}$ are optimum. However, f must be *smooth* [8], otherwise, the paths may not be optimum.

The cost of a trivial path $\pi_t = \langle t \rangle$ is usually based on a seed set \mathcal{S} , and the cost for non-trivial paths follow a path-extension rule. The function $f_{\max}^{\|\mathcal{S}\|}$ is one example of smooth function [8], which will be important in COIFT. Note that $f_{\max}^{\|\mathcal{S}\|}$ processes anti-parallel arcs $\langle t, s \rangle$ along the path, which requires a symmetric digraph.

$$f_{\max}^{\|\mathcal{S}\|}(\langle t \rangle) = \begin{cases} -1 & \text{if } t \in \mathcal{S} \\ +\infty & \text{otherwise} \end{cases}$$

$$f_{\max}^{\|\mathcal{S}\|}(\pi_s \cdot \langle s, t \rangle) = \max\{f_{\max}^{\|\mathcal{S}\|}(\pi_s), \omega(\langle t, s \rangle)\} \quad (1)$$

Algorithm 1 computes a path-cost map V , which converges to V_{opt}^f if f is a smooth function [8]. It is also optimized in handling infinite costs, by storing in \mathcal{Q} only the nodes with finite-cost path, assuming that $V_{opt}^f(t) < +\infty$ for all $t \in \mathcal{V}$.

Algorithm 1. – IFT ALGORITHM

INPUT: Image graph $G = \langle \mathcal{V}, \mathcal{A}, \omega \rangle$, and function f .
 OUTPUT: Optimum-path forest P and the path-cost map V .
 AUXILIARY: Priority queue \mathcal{Q} , variable tmp , and set \mathcal{F} .

1. **For each** $t \in \mathcal{V}$, **do**
2. Set $P(t) \leftarrow nil$, $V(t) \leftarrow f(\langle t \rangle)$ and $\mathcal{F} \leftarrow \emptyset$.
3. **If** $V(t) \neq +\infty$, **then** insert t in \mathcal{Q} .
4. **While** $\mathcal{Q} \neq \emptyset$, **do**
5. Remove s from \mathcal{Q} such that $V(s)$ is minimum.
6. Add s to \mathcal{F} .
7. **For each** pixel t such that $\langle s, t \rangle \in \mathcal{A}$ and $t \notin \mathcal{F}$, **do**
8. Compute $tmp \leftarrow f(\pi_s^P \cdot \langle s, t \rangle)$.
9. **If** $tmp < V(t)$, **then**
10. **If** $V(t) \neq +\infty$, **then** remove t from \mathcal{Q} .
11. Set $P(t) \leftarrow s$, $V(t) \leftarrow tmp$.
12. Insert t in \mathcal{Q} .

B. Oriented Image Foresting Transform (OIFT)

Let G be a strongly connected and symmetric digraph, where the weights $\omega(\langle s, t \rangle)$ are a combination of an undirected dissimilarity measure $\delta(\langle s, t \rangle)$ between neighboring pixels s and t , multiplied by an orientation factor, as follows:

$$\omega(\langle s, t \rangle) = \begin{cases} \delta(\langle s, t \rangle) \times (1 + \alpha) & \text{if } I(s) > I(t) \\ \delta(\langle s, t \rangle) \times (1 - \alpha) & \text{if } I(s) < I(t) \\ \delta(\langle s, t \rangle) & \text{otherwise} \end{cases} \quad (2)$$

where $\alpha \in [-1, 1]$. Different procedures can be adopted for $\delta(\langle s, t \rangle)$, as discussed in [18], [19], such as the absolute value of the difference of image intensities (i.e., $\delta(\langle s, t \rangle) = |I(s) - I(t)|$). Note that we usually have $\omega(\langle s, t \rangle) \neq \omega(\langle t, s \rangle)$ when $\alpha \neq 0$. For colored images, a reference map should be considered for $I(t)$ in Eq. 2, or α must be set to zero [17].

OIFT is build upon the IFT framework by considering the following path function in a symmetric digraph:

$$\begin{aligned} f^\sigma(\langle t \rangle) &= \begin{cases} -1 & \text{if } t \in \mathcal{S}_1 \cup \mathcal{S}_0 \\ +\infty & \text{otherwise} \end{cases} \\ f^\sigma(\pi_{r \rightsquigarrow s} \cdot \langle s, t \rangle) &= \begin{cases} \omega(\langle s, t \rangle) & \text{if } r \in \mathcal{S}_1 \\ \omega(\langle t, s \rangle) & \text{otherwise} \end{cases} \end{aligned} \quad (3)$$

where \mathcal{S}_1 and \mathcal{S}_0 denote, respectively, the set of seeds selected inside and outside the object to be segmented.

The segmented object \mathcal{O}^P by OIFT is defined from the forest P computed by Algorithm 1, with f^σ , by taking as object pixels the set of pixels that were conquered by paths rooted in \mathcal{S}_1 , i.e., $\mathcal{O}^P = \{t \in \mathcal{V} \mid \pi_t^P = \tau_{\mathcal{S}_1 \rightsquigarrow t}\}$. For $\alpha > 0$, the segmentation by OIFT favors transitions from bright to dark pixels, and $\alpha < 0$ favors the opposite orientation.

The function f^σ is a non-smooth connectivity function, as described in [17]. The optimality of \mathcal{O}^P by OIFT is supported by an energy criterion of cut in graphs involving arcs

from object to background pixels $\mathcal{C}(\mathcal{O}^P)$ (outer-cut boundary), according to Theorem 1 from [16], [17].

$$\mathcal{C}(\mathcal{O}) = \{\langle s, t \rangle \in \mathcal{A} \mid s \in \mathcal{O} \text{ and } t \notin \mathcal{O}\} \quad (4)$$

$$E(\mathcal{O}) = \min_{(s,t) \in \mathcal{C}(\mathcal{O})} \omega(\langle s, t \rangle) \quad (5)$$

Theorem 1 (Outer-cut optimality by OIFT). *For two given sets of seeds \mathcal{S}_1 and \mathcal{S}_0 , let $\mathcal{U}(\mathcal{S}_1, \mathcal{S}_0) = \{\mathcal{O} \subseteq \mathcal{V} \mid \mathcal{S}_1 \subseteq \mathcal{O} \subseteq \mathcal{V} \setminus \mathcal{S}_0\}$ denote the universe of all possible objects satisfying the seed constraints. Any spanning forest P computed by Algorithm 1 for function f^σ defines a segmented object \mathcal{O}^P that maximizes E (Eq. 5) among all possible segmentation results in \mathcal{U} . That is, $E(\mathcal{O}^P) = \max_{\mathcal{O} \in \mathcal{U}(\mathcal{S}_1, \mathcal{S}_0)} E(\mathcal{O})$.*

III. OIFT WITH CONNECTIVITY CONSTRAINTS

In [13], a new method that incorporates connectivity constraints has been proposed in the OIFT approach, named *Connected Oriented Image Foresting Transform* (COIFT), which avoids the generation of segmentations with disconnected regions. In this section, we show that COIFT can be extended by introducing a new parameter that controls the width of the connectivity regions, making it more adaptable to different objects (see Figure 2).

Let $\mathcal{U}_C(\mathcal{S}_1, \mathcal{S}_0)$ be the set of all connected objects satisfying the seed constraints, defined as $\mathcal{U}_C(\mathcal{S}_1, \mathcal{S}_0) = \{\mathcal{O} \in \mathcal{U}(\mathcal{S}_1, \mathcal{S}_0) \mid G[\mathcal{O}] \text{ is strongly connected}\}$, where $G[\mathcal{O}]$ is the subgraph of G induced by \mathcal{O} . COIFT maximizes the energy E (Equation 5) in a strongly connected and symmetric digraph G among all connected objects in $\mathcal{U}_C(\mathcal{S}_1, \mathcal{S}_0)$.

Let $E_A = \max_{\mathcal{O} \in \mathcal{U}(A, \mathcal{S}_0)} E(\mathcal{O})$ denote the optimum energy value using set A as internal seeds. According to the same notation, $E_{\{t\}}$ denotes the optimum energy from a single internal seed t , when $\mathcal{S}_1 = \{t\}$.

The COIFT prior is supported by the following propositions.

Proposition 1. *Let $E_{A \cup B}$ be the energy of a seed set $A \cup B$. The optimum energy $E_{A \cup B}$ among all objects in $\mathcal{U}(A \cup B, \mathcal{S}_0)$, satisfies $E_{A \cup B} = \min\{E_A, E_B\}$.*

Proposition 2. *For a given strongly connected and symmetric digraph G , and sets of seeds \mathcal{S}_1 and \mathcal{S}_0 , such that $\mathcal{S}_1 = \{t\}$ we have that $E_{\{t\}} = V_{opt}^{f_{\max}^{\mathcal{S}_0}}(t)$.*

Where $V_{opt}^{f_{\max}^{\mathcal{S}_0}}(t)$ is the cost of an optimum path by function $f_{\max}^{\mathcal{S}_0}$ (Eq. 1).

Proposition 1 has been proven in [13], and the proof of Proposition 2 follows immediately from Lemma 1 in [20], which shows it in its dual form.

Now, by extending COIFT we consider a disk with center in t and adjacency radius γ , which represents the set of all pixels within it, denoted by

$$\mathcal{V}_\circ(t, \gamma) = \{x \in \mathcal{V} \mid \|t - x\| \leq \gamma\} \quad (6)$$

where $\|t - x\|$ represents the Euclidean distance between pixels t and x . Note that $x = t$ is also in $\mathcal{V}_\circ(t, \gamma)$.

We also denote $E_{\mathcal{V}_\circ(t, \gamma)}$ as the optimum energy from $\mathcal{S}_1 = \mathcal{V}_\circ(t, \gamma)$, considering a disk $\mathcal{V}_\circ(t, \gamma)$.

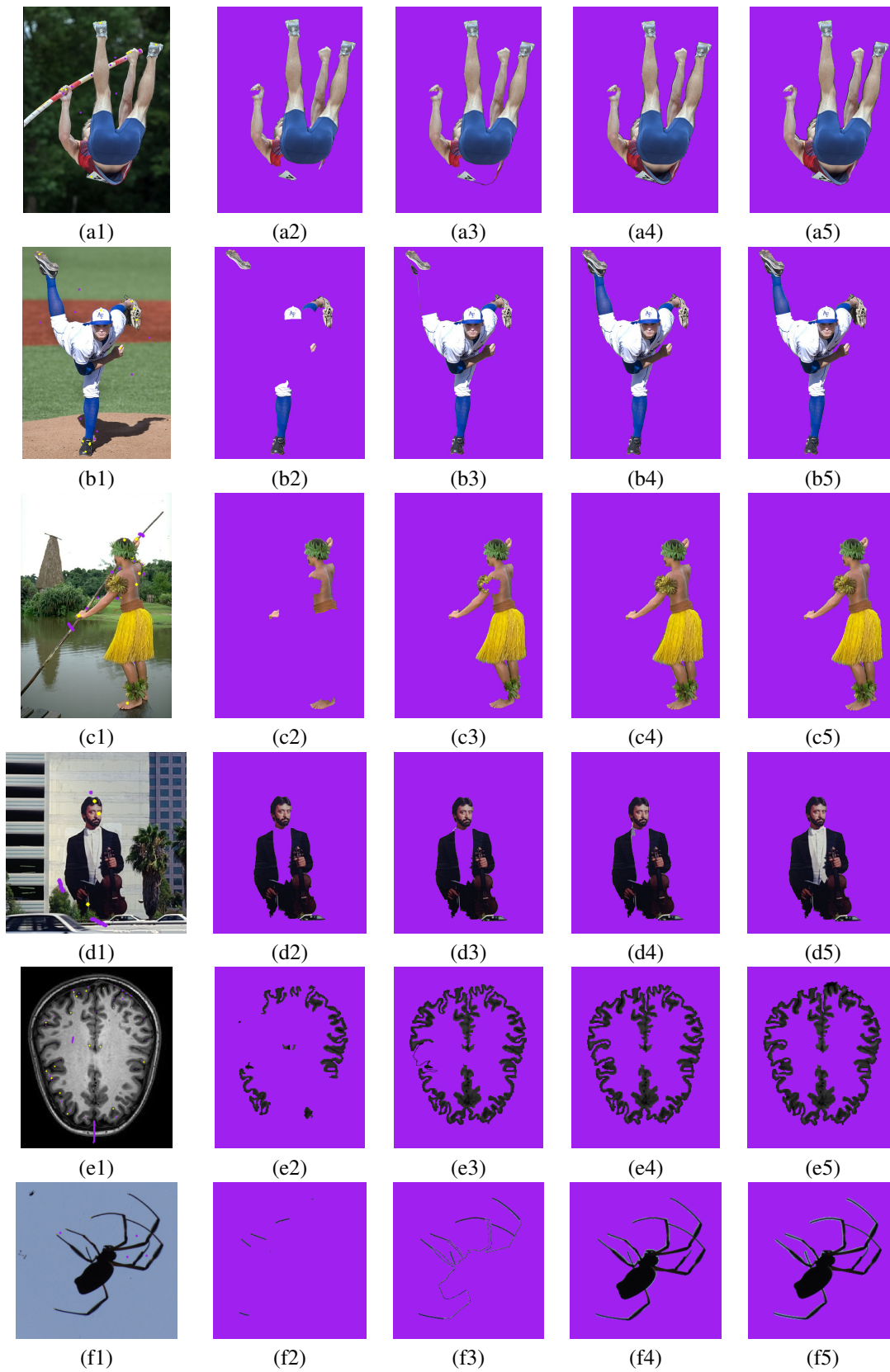


Fig. 2. The first column represents the input images with user-selected markers. The second column, segmentations without connectivity constraints (OIFT with $\alpha = 0.0$). The third column, segmentations with COIFT ($\alpha = 0.0$ and $\gamma = 0.0$). The fourth column, segmentations with COIFT ($\alpha = 0.0$ and $\gamma = 1.0$). The fifth column, segmentations with COIFT ($\alpha = 0.0$ and $\gamma = 2.0$). The proposed results by COIFT guarantee connected objects.

Hence, COIFT comprises the following steps: **1)** Compute $E_{\mathcal{V}_\ominus(t,\gamma)}$ for all $t \in \mathcal{V}$. **2)** Secondly, we must interconnect disconnected seeds in \mathcal{S}_1 , by computing paths passing through pixels s with maximum energy $E_{\mathcal{V}_\ominus(t,\gamma)}$, resulting in a new connected set of internal seeds \mathcal{S}_1^C . **3)** Execute the OIFT method with f^σ from seed sets \mathcal{S}_1^C and \mathcal{S}_0 , generating a final connected result.

The main difference in relation to the original COIFT resides in the Steps 1 and 2 where we have to compute $E_{\mathcal{V}_\ominus(t,\gamma)}$ instead of $E_{\{t\}}$ (see Figure 3).

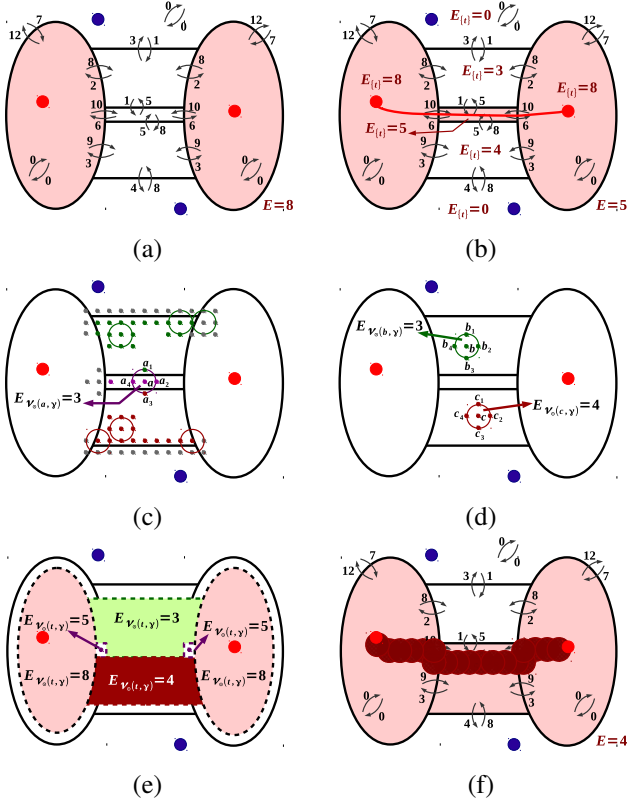


Fig. 3. Graph representation with segmentations results by: (a) OIFT. (b) COIFT ($\gamma = 0$), the riverbed path interconnecting the seeds and the values of $E_{\{t\}}$ for each region are shown in red. (c-f) COIFT with $\gamma = 1.0$. In (c-d), we can observe how the energy of the disks is computed for the pixels a , b and c , i.e., $E_{\mathcal{V}_\ominus(a,\gamma)} = \min\{E_{\{a_1\}}, E_{\{a_2\}}, E_{\{a_3\}}, E_{\{a_4\}}, E_{\{a\}}\} = \min\{3, 5, 4, 5, 5\} = 3$, $E_{\mathcal{V}_\ominus(b,\gamma)} = \min\{E_{\{b_1\}}, E_{\{b_2\}}, E_{\{b_3\}}, E_{\{b_4\}}, E_{\{b\}}\} = \min\{3, 3, 3, 3, 3\} = 3$ and $E_{\mathcal{V}_\ominus(c,\gamma)} = \min\{E_{\{c_1\}}, E_{\{c_2\}}, E_{\{c_3\}}, E_{\{c_4\}}, E_{\{c\}}\} = \min\{4, 4, 4, 4, 4\} = 4$. The colored regions in (e) represent the final energy regions $E_{\mathcal{V}_\ominus(t,\gamma)}$ for all $t \in \mathcal{V}$. (f) The riverbed path interconnecting the seeds.

Consider $\mathcal{V}_\ominus(t,\gamma) = \{x_1, x_2, \dots, x_m\}$, where m is the number of pixels within the disk $\mathcal{V}_\ominus(t,\gamma)$, including t . From Proposition 1 we can conclude that

$$E_{\mathcal{V}_\ominus(t,\gamma)} = \min_{x \in \mathcal{V}_\ominus(t,\gamma)} \{E_{\{x\}}\}$$

and by Proposition 2, we also have that

$$E_{\mathcal{V}_\ominus(t,\gamma)} = \min_{x \in \mathcal{V}_\ominus(t,\gamma)} \{V_{opt}^{f_{max}^{S_0}}(x)\}$$

Consequently, the first step of COIFT can be accomplished by computing the erosion of $V_{opt}^{f_{max}^{S_0}}$ with erosion radius γ . We first compute $V_{opt}^{f_{max}^{S_0}}$ for all $t \in \mathcal{V}$, which requires one execution of Algorithm 1 with $f_{max}^{S_0}$, using only the external seeds in \mathcal{S}_0 and then compute the erosion of the cost map $V_{opt}^{f_{max}^{S_0}}(t)$.

In the second step, we interconnect disconnected seeds in \mathcal{S}_1 through pixels t centered in disks $\mathcal{V}_\ominus(t,\gamma)$ with higher energy values $E_{\mathcal{V}_\ominus(t,\gamma)}$, in order to get the best connected result with the given width parameter γ according to Proposition 1. We consider a particular case of the cost function employed by the *Riverbed* method [21].

$$f_{river}(\cdot(t)) = \begin{cases} -1 & \text{if } t = s^* \\ +\infty & \text{otherwise} \end{cases}$$

$$f_{river}(\pi_s \cdot \langle s, t \rangle) = K - E_{\mathcal{V}_\ominus(t,\gamma)} \quad (7)$$

where $K = \max_{t \in \mathcal{V}} E_{\mathcal{V}_\ominus(t,\gamma)}$ and s^* is a given starting point.

A riverbed path $\tau_{r \rightsquigarrow t}$ (computed by Algorithm 1 using f_{river}) from pixel $r = s^*$ to t , always traverses a sequence of intermediary pixels t_i , for which the maximum value of $K - E_{\mathcal{V}_\ominus(t_i,\gamma)}$ along any part of it is minimized among other possible alternative routes [21]. Consequently, a riverbed path by f_{river} always seeks higher levels of $E_{\mathcal{V}_\ominus(t_i,\gamma)}$ as desired (Figure 3). We select an arbitrary node in \mathcal{S}_1 to use as s^* , and then compute one IFT with f_{river} generating a forest P . For all $t \in \mathcal{S}_1$, such that $t \neq s^*$, we select all pixels t_i in the path π_t^P , including the pixels in their disks $\mathcal{V}_\ominus(t_i,\gamma)$ (Figure 3f), to compose a new connected set of internal seeds \mathcal{S}_1^C .

In the last step, we simply compute the OIFT method with f^σ from seed sets \mathcal{S}_1^C and \mathcal{S}_0 , generating a final result, which is guaranteed to be a connected object.

A. Handling ties in the energy formulation

Whenever the segmentation by OIFT is already resulting in a single connected component, we would expect that COIFT produces the same result. However, in cases where there are multiple solutions with the same optimum energy values, COIFT could select an alternative connection path by riverbed, leading to a different segmentation, as illustrated in Figure 4. In order to guarantee the same output in these cases, we change the riverbed function to favor the selection of connection paths that pass through the OIFT segmentation, by assigning the lowest cost to pixels in the OIFT result.

B. Connectivity Constraints for background seeds

The connectivity constraint can also be applied for the background seeds to guarantee connected backgrounds. In order to accomplish this goal, we need to invert the roles played by the internal and external seeds and apply COIFT in the transpose graph G^T , as illustrated in Figure 5. Note that in this case we guarantee segmented objects without holes.

IV. EXPERIMENTS

We compared COIFT against other methods with competitive running times (OIFT [16], ORFC+GC [20], [22]), to show

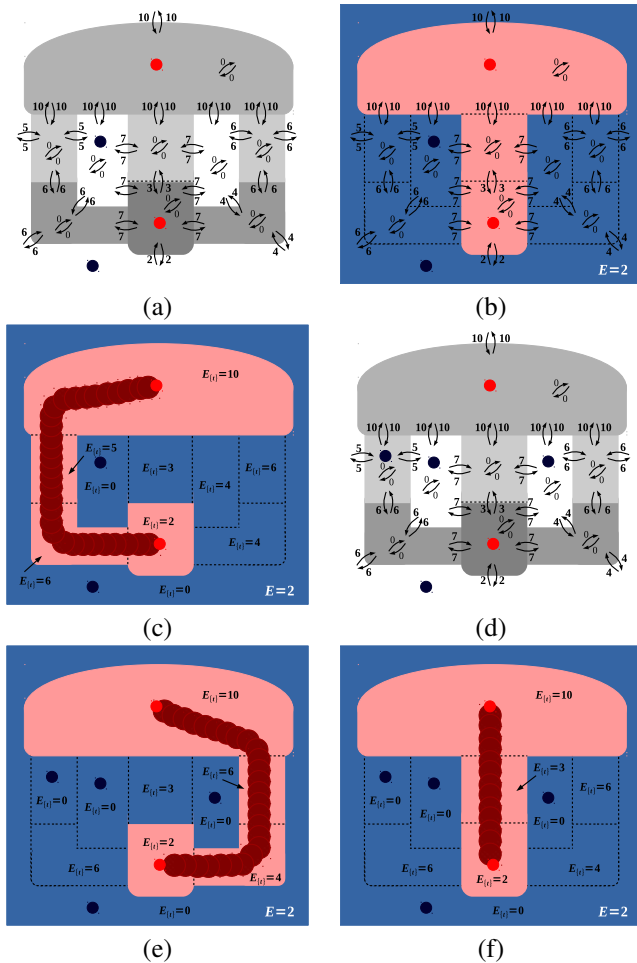


Fig. 4. (a) Schematic representation of a synthetic image with internal (red markers) and external (blue markers) seeds. (b) OIFT result. (c) COIFT result. The values of $E_{\{t\}}$ for each region are shown. (d) Additional external seeds are selected. (e) Updated result by COIFT. Note that even with more external seeds COIFT still does not give the same solution of OIFT, which has a single connected component. (f) COIFT result considering the modified riverbed function that favors pixels in OIFT. Note that the results in (c), (e) and (f) have the same energy (i.e., $E = 2$). For COIFT results, the riverbed path interconnecting the internal seeds is shown in red.

how ε_{∞} -minimization (or equivalently $E(\mathcal{O})$ -maximization) based methods can benefit from the use of connectivity constraints. In order to stress the methods, we only considered the image-based weight assignment from [19] for $\delta(s, t)$ in Equation 2, without any prior intensity distribution model, aiming a higher challenge. The experiments were conducted using a robot user, as proposed by Gulshan et al. [23], to simulate user interaction by placing brush strokes automatically to iteratively perform the segmentation task.

In our experiments we used two image datasets, one composed by natural images and the other by MRT1 images. In the first experiment, we used 50 public images of birds ¹ (Figure 6). The ground truth for these images was generated by manual segmentation and it is publicly available to the com-

¹ These images are released under Creative Commons CC0 into the public domain, available at the web site <https://pixabay.com/>.

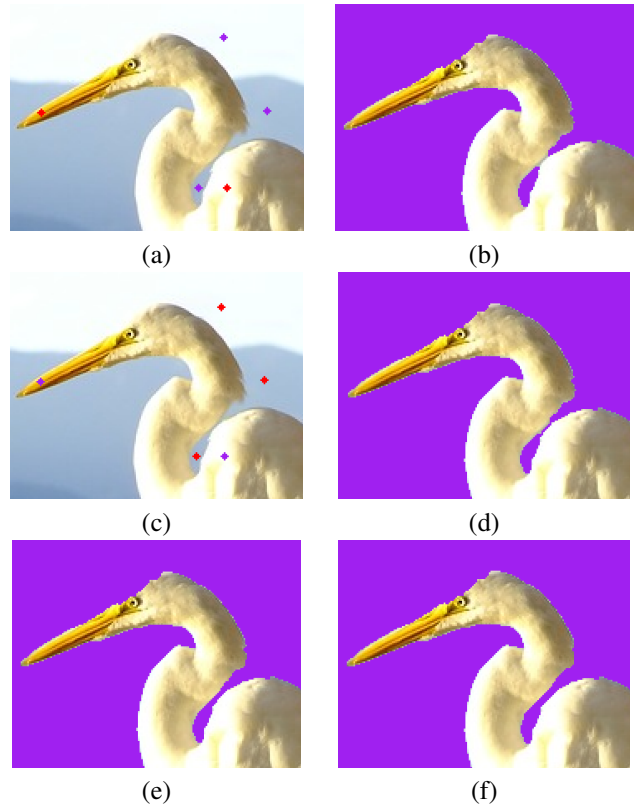


Fig. 5. (a) Input image with user-selected markers. (b) Segmentation without connectivity constraints (OIFT with $\alpha = 0.0$). (c) Inverted markers of the image (a). (d) Segmentation with COIFT ($\alpha = 0.0$ and $\gamma = 0.0$). (e) Segmentation with COIFT ($\alpha = 0.0$ and $\gamma = 1.0$). (f) Segmentation with COIFT ($\alpha = 0.0$ and $\gamma = 2.0$). The proposed results by COIFT guarantee connected backgrounds.

munity ². Figure 6 shows segmentation results by OIFT [16] and COIFT with different radius values γ for the same user-selected markers, making clear the advantages of COIFT. Note that the dataset contains objects with thin and elongated parts. In Figure 7 we show the mean error curves using a robot user for segmenting the bird dataset. For each segmentation, the error was computed as the mean distance of the ground truth boundary from the delineated boundary. ORFC+GC [20], [22] did not perform well in this dataset because it was not able to segment some thin and elongated parts of the objects.

In the second experiment, we used 44 MRT1-images of phantoms (available at the BrainWeb site ³) to segment the cortical gray matter (Figure 8). Figure 9 shows the mean error curves for all the images using a robot user for the segmentation of the cortical gray matter. Note that COIFT has the lowest error among all approaches for $\gamma = 2.0$.

V. CONCLUSION

In this work, we extended COIFT to support a user-controllable minimum width of the connectivity constraint. It includes the method by Mansilla et al. [13] as a particular

²URL: <http://vision.ime.usp.br/~lucyacm/datasets/birds.html>.

³URL: <http://www.bic.mni.mcgill.ca/brainweb/>

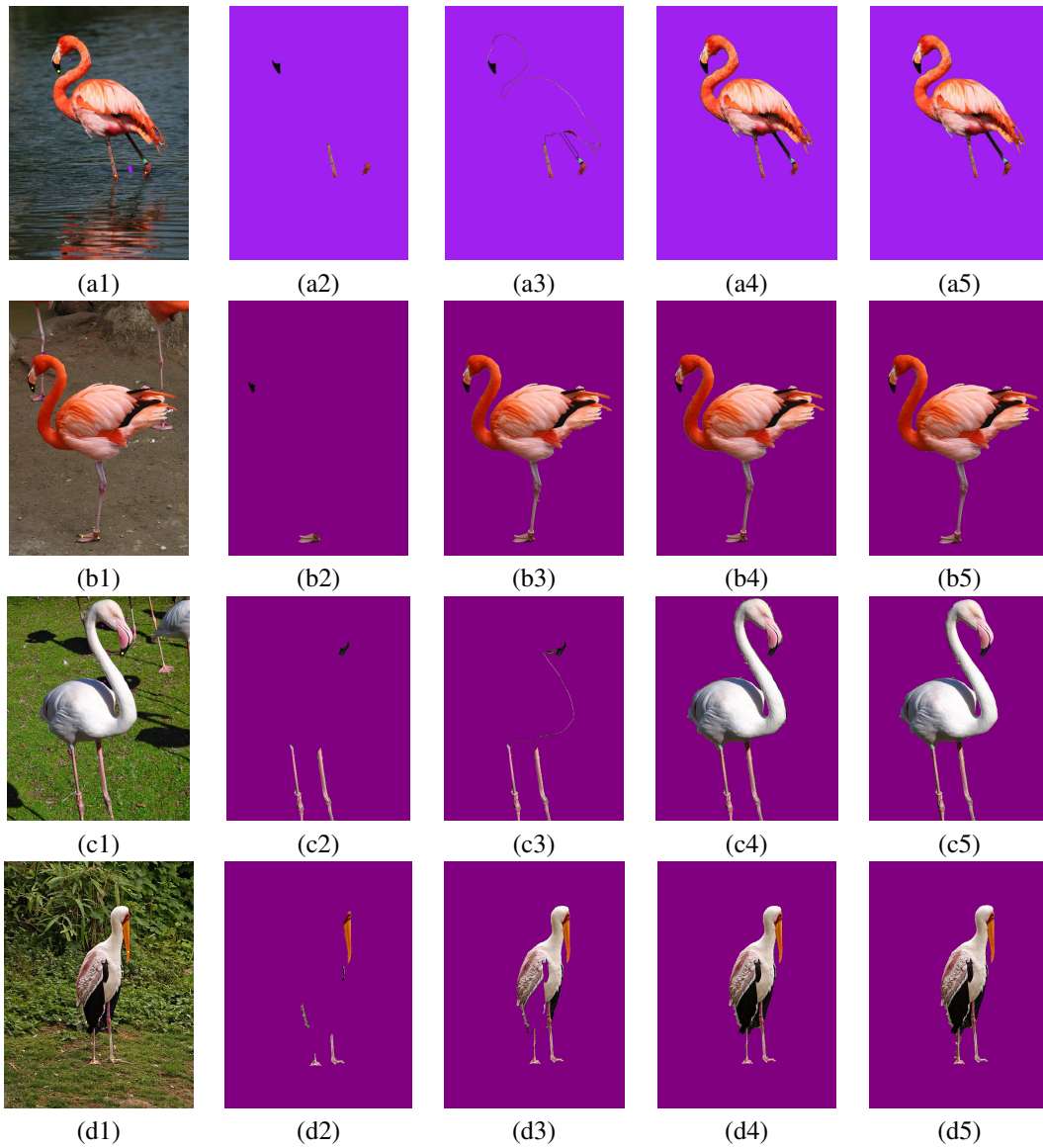


Fig. 6. Segmentation of different birds: The first column represents the input images with user-selected markers. The second column, segmentations without connectivity constraints (OIFT with $\alpha = 0.0$). The third column, segmentations with COIFT ($\alpha = 0.0$ and $\gamma = 0.0$). The fourth column, segmentations with COIFT ($\alpha = 0.0$ and $\gamma = 1.0$). The fifth column, segmentations with COIFT ($\alpha = 0.0$ and $\gamma = 2.0$). The proposed results by COIFT guarantee connected objects.

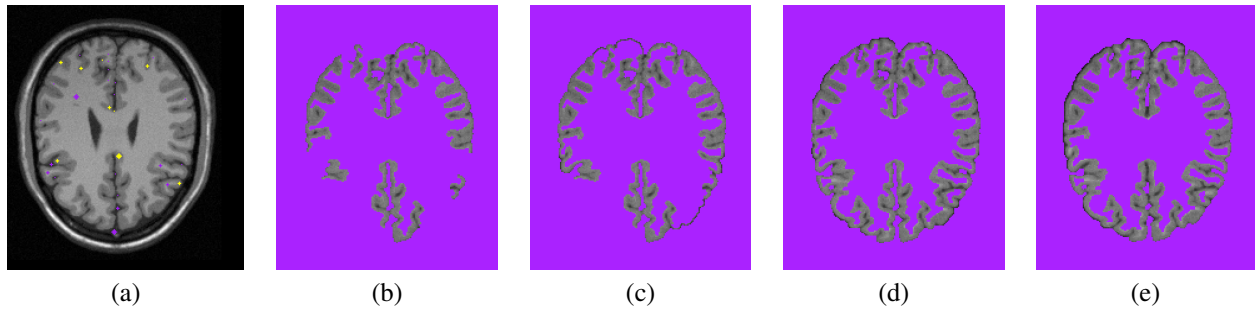


Fig. 8. Segmentation of the cortical gray matter: (a) The input image with user-selected markers. (b) Segmentation without connectivity constraints (OIFT with $\alpha = 0.0$). (c) Segmentation by COIFT with $\alpha = 0.0$ and $\gamma = 0.0$. (d) Segmentation by COIFT with $\alpha = 0.0$ and $\gamma = 1.0$. (e) Segmentation by COIFT with $\alpha = 0.0$ and $\gamma = 2.0$. The proposed results by COIFT guarantee connected objects.

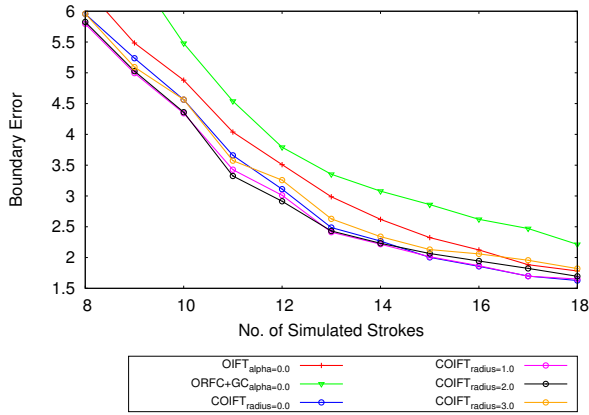


Fig. 7. The mean error curve (boundary error) using a robot user for segmenting the bird dataset.

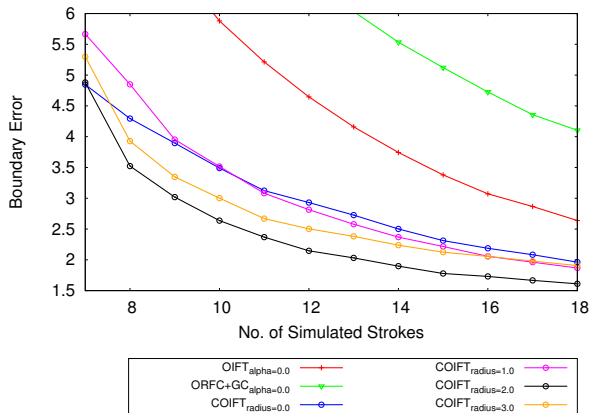


Fig. 9. The mean error curve (boundary error) using a robot user for the segmentation of the cortical gray matter.

case when $\gamma = 0.0$. We also improved the handling of ties in COIFT energy formulation and discussed its application to avoid objects with holes, by applying the connectivity constraint for the background seeds.

The new method, successfully incorporates connectivity constraints on OIFT, preserving its low time complexity $O(N = |\mathcal{V}|)$ (when \mathcal{Q} is implemented using bucket sorting [8]), since it requires only four executions of Algorithm 1.

Connectivity constraints are especially helpful on 3D applications involving connected objects with thin parts, such as a vascular network. As future work, we intend to test COIFT in a full automatic segmentation framework.

ACKNOWLEDGMENT

Thanks to CNPq (308985/2015-0, 305381/2012-1, 486083/2013-6, FINEP 1266/13), FAPESP grant # 2011/50761-2, CNPq, CAPES, and NAP eScience - PRP - USP for funding.

REFERENCES

[1] L. Grady, "Random walks for image segmentation," *IEEE Trans. Pattern Analysis and Machine Intelligence*, vol. 28, no. 11, pp. 1768–1783, 2006.

[2] Y. Boykov and G. Funka-Lea, "Graph cuts and efficient N-D image segmentation," *Intl. Jnl. of Comp. Vision*, vol. 70, no. 2, pp. 109–131, 2006.

[3] X. Bai and G. Sapiro, "Distance cut: Interactive segmentation and matting of images and videos," in *Proc. of the IEEE Intl. Conf. on Image Processing*, vol. 2, 2007, pp. II – 249–II – 252.

[4] K. Ciesielski, J. Udupa, P. Saha, and Y. Zhuge, "Iterative relative fuzzy connectedness for multiple objects with multiple seeds," *Computer Vision and Image Understanding*, vol. 107, no. 3, pp. 160–182, 2007.

[5] J. Cousty, G. Bertrand, L. Najman, and M. Couprie, "Watershed cuts: Thinnings, shortest path forests, and topological watersheds," *Trans. on Pattern Analysis and Machine Intelligence*, vol. 32, pp. 925–939, 2010.

[6] K. Ciesielski, J. Udupa, A. Falcão, and P. Miranda, "A unifying graph-cut image segmentation framework: algorithms it encompasses and equivalences among them," in *Proc. of SPIE on Medical Imaging: Image Processing*, vol. 8314, 2012.

[7] C. Couprie, L. Grady, L. Najman, and H. Talbot, "Power watersheds: A unifying graph-based optimization framework," *IEEE Transactions on Pattern Analysis and Machine Intelligence*, vol. 99, no. 7, pp. 1384–1399, Jul 2010.

[8] A. Falcão, J. Stolfi, and R. Lotufo, "The image foresting transform: Theory, algorithms, and applications," *IEEE Transactions on Pattern Analysis and Machine Intelligence*, vol. 26, no. 1, pp. 19–29, 2004.

[9] O. Lézoray and L. Grady, *Image Processing and Analysis with Graphs: Theory and Practice*. California, USA: CRC Press, 2012.

[10] S. Vicente, V. Kolmogorov, and C. Rother, "Graph cut based image segmentation with connectivity priors," in *Computer Vision and Pattern Recognition, 2008. CVPR 2008. IEEE Conf. on*, June 2008, pp. 1–8.

[11] Y. Zeng, D. Samaras, W. Chen, and Q. Peng, "Topology cuts: A novel min-cut/max-flow algorithm for topology preserving segmentation in nd images," *Computer Vision and Image Understanding*, vol. 112, no. 1, pp. 81 – 90, 2008, special Issue on Discrete Optimization in Computer Vision. [Online]. Available: <http://www.sciencedirect.com/science/article/pii/S1077314208001094>

[12] S. Nowozin and C. H. Lampert, "Global interactions in random field models: A potential function ensuring connectedness," *SIAM Journal on Imaging Sciences*, vol. 3, no. 4, pp. 1048–1074, 2010. [Online]. Available: <http://dx.doi.org/10.1137/090752614>

[13] L. Mansilla, P. Miranda, and F. Cappabianco, "Oriented image foresting transform segmentation with connectivity constraints," in *Image Processing (ICIP), 23rd IEEE Intl. Conf. on*, Sept 2016, accepted to appear.

[14] L. Mansilla, M. Jackowski, and P. Miranda, "Image foresting transform with geodesic star convexity for interactive image segmentation," in *Image Processing (ICIP), 20th IEEE Intl. Conf. on*, Sept 2013, pp. 4054–4058.

[15] C. de Moraes Braz and P. Miranda, "Image segmentation by image foresting transform with geodesic band constraints," in *Image Processing (ICIP), 2014 IEEE Intl. Conf. on*, Oct 2014, pp. 4333–4337.

[16] P. Miranda and L. Mansilla, "Oriented image foresting transform segmentation by seed competition," *IEEE Transactions on Image Processing*, vol. 23, no. 1, pp. 389–398, Jan 2014.

[17] L. Mansilla and P. Miranda, "Image segmentation by oriented image foresting transform: Handling ties and colored images," in *18th Intl. Conf. on Digital Signal Processing*, Greece, Jul 2013, pp. 1–6.

[18] K. Ciesielski and J. Udupa, "Affinity functions in fuzzy connectedness based image segmentation i: Equivalence of affinities," *Computer Vision and Image Understanding*, vol. 114, no. 1, pp. 146–154, Jan 2010.

[19] P. Miranda, A. Falcão, and J. Udupa, "Synergistic arc-weight estimation for interactive image segmentation using graphs," *Computer Vision and Image Understanding*, vol. 114, no. 1, pp. 85–99, Jan 2010.

[20] H. H. Bejar and P. A. Miranda, "Oriented relative fuzzy connectedness: Theory, algorithms, and its applications in hybrid image segmentation methods," *EURASIP Journal on Image and Video Processing*, vol. 2015, no. 21, Jul 2015.

[21] P. Miranda, A. Falcao, and T. Spina, "Riverbed: A novel user-steered image segmentation method based on optimum boundary tracking," *Image Processing, IEEE Transactions on*, vol. 21, no. 6, pp. 3042–3052, June 2012.

[22] K. C. Ciesielski, P. Miranda, A. Falcão, and J. K. Udupa, "Joint graph cut and relative fuzzy connectedness image segmentation algorithm," *Medical Image Analysis (MEDIA)*, vol. 17, no. 8, pp. 1046–1057, 2013.

[23] V. Gulshan, C. Rother, A. Criminisi, A. Blake, and A. Zisserman, "Geodesic star convexity for interactive image segmentation," in *Proc. of Computer Vision and Pattern Recognition*, 2010, pp. 3129–3136.